Health Management and Diagnostics for Synthetic Aperture Radar (SAR) Payloads

Gregory Bower[1], Jonathan Zook[1] and Ross Bird[1]

[1]*QorTek Inc., Williamsport, PA, 17701*

gbower@qortek.com
jzook@qortek.com
rbird@qortek.com

ABSTRACT

A statistical method based on symbolic analysis is presented for health management of Synthetic Aperture Radar systems. The approach, based on symbolic theory, develops statistical models of the underlying system dynamics using an underlying Markov assumption and tracks the change in model over time to determine system health. The methodology was designed for minimal impact to legacy systems and required minimal computational effort in order to operate at radar data rates. The approach was applied to radar phase history data corrupted with simulated degradation. Two degradation mechanisms were studied: interference and array degradation. In addition, the results of combined degradation were also studied in this work.

1. INTRODUCTION

Health management of systems can result in the reduction of necessary man-hours and costs associated with maintenance of equipment. In addition, a health management routine can be used to determine the remaining useful life of a system and to determine when to schedule upcoming repairs. Data driven methods utilize data captured in real-time from the system in order to determine the current state of health of the system. Data driven methods form underlying models of the system using this captured time series data. These underlying models developed through operation of the system can then be used to quantify remaining health.

The method was originally applied to monitoring the health of a dc-dc forward converter in order to predict the remaining useful life of the converter (Bower, Mayer, & Reichard, 2011)(Bower, Mayer, Reichard, 2008). The Markov assumption is implied for the system under investigation from which statistical models are developed and tracked through time. Increasing degradation results in perturbing the operational characteristics of the system which can result in a shift in the Markov process (Papoulis & Pillai, 2002). This shift can be quantifiable and with proper training, predictable in the future for prognostic purposes.

In this work, a symbolic approach was adopted for health monitoring of imaging radar payloads on Unmanned Aerial Vehicles (UAVs). These radar platforms are complex systems difficult to model classically which makes the proposed data based approach ideal for health monitoring. The primary objective of this research was to determine the feasibility of applying such a method to the high data rates seen in an imaging radar platform which is a product of the pulse repetition rate of the radar at the desired sample rate and bandwidth of the return echoes. In addition, the approach cannot interfere with the operation of the platform or radar system. The methodology was tested with radar phase history data and two common issues with imaging radars, interference and array degradation were investigated. The results are also expected to lead to an ability to discriminate between the two degradation mechanisms to assist in optimizing the operation of the radar payload. This paper begins with a discussion on the Symbolic Analysis approach specifically applied to the imaging radar payload and all details of the approach are discussed. In Section III, a brief review of Synthetic Aperture Radar and radar platforms is completed. Section IV reviews the results obtained from the simulations and feasibility testing of the approach and the paper concludes with future work in Section V.

2. SYMBOLIC ANALYSIS

Symbolic Analysis is a statistical pattern recognition tool based upon symbolic theory. Most work in the symbolic realm deals with the development of optimal models to determine the trajectory of modeled system states (Daw, Finney & Tracy, 2003). These methods are used to model complex and chaotic systems. The resultant optimal model, known as the ε machine, has a variable dimensional structure whose dimensions were constantly adjusted depending on the data collected over time. This variation in dimensionality made it difficult to determine deviations

between models developed through system usage. In order to make meaningful comparisons between models, a machine was developed with a-priori fixed dimensional structure (Ray, 2004). This fixed dimensional machine allows for meaningful comparisons between statistical models defined at different temporal points in the system's life at the cost of optimality. Using the SA approach, it is possible to generate a measure that quantifies the amount of degradation within a recorded observable. The process of SA is shown in the block diagram of Figure 1. The basic methodology requires four steps which will be detailed in the next sections.

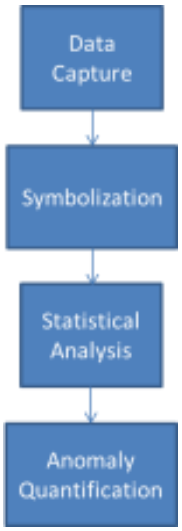

Figure 1. Symbolic analysis of time series data block diagram.

2.1. **Data Capture**

Although the process of data capture might seem straightforward, the process requires some careful consideration. First, the type of data and where it is captured must be known. This entails the study of the underlying system in order to determine the common failure points of the system. Once these failure points are known, the rate and length of the data to be recorded must be determined.

Symbolic analysis requires two assumptions. First, it was assumed that the degradation within the system monotonically increases. This means that the system does not undergo 'self-healing' or is repaired during the monitoring process. Limiting self-healing is important for the implementation of remaining health estimation. Secondly, it was assumed that the degradation mechanisms act slower than the system dynamics. This assumptions states that when the system is observed and the time series data collected, that the degradation in the system during this period was assumed to be constant. In this manner, a model of the system was developed based on the constant state of degradation.

For the application to radar platforms, specifically SAR systems, the data implemented in the algorithm was the fast time scale which was developed from an individual pulse (phase history data). The slow time scale was defined to be the pulse rate or repetition rate of the platform.

2.2. **Symbolization**

The next step involves transforming the time series data into the symbolic domain. This step can be thought of as a general re-quantization of the original data resulting in a coarser distribution. Symbolization requires the determination of the number of partitions to be used as well as the type of partitioning. The two most common types of partitioning include uniform partitioning (UP) and maximum entropy (ME) partitioning. The choice in the number of partitions will depend on the time series data being analyzed as well as the type of degradation and features to be analyzed.

The partitioning was kept invariant over the entire monitoring period such that the statistical models developed later in the system life can be directly compared to the baseline. The baseline model was defined on the healthy state of the system.

2.3. **Uniform Partitioning**

Uniform partitioning divides the range of the time series data into equal sized regions where the total number of determined partitions are defined as the set P. Given the range of the time series data as U, the partition sizes are defined as U/P and the boundaries developed from the range U. Each partition region P_i was mutually exclusive and exhaustive over the range of the data. The probabilities of the partition occurrence in the uniform case are not necessarily equal; however, the partitioning structure was equal.

To construct UP, the maximum and minimum of the time series data were evaluated and the resultant range was divided equally into P regions. These regions are assigned a unique symbol to complete the partition description. An example of UP on a sinusoidal waveform is shown in Figure 2.

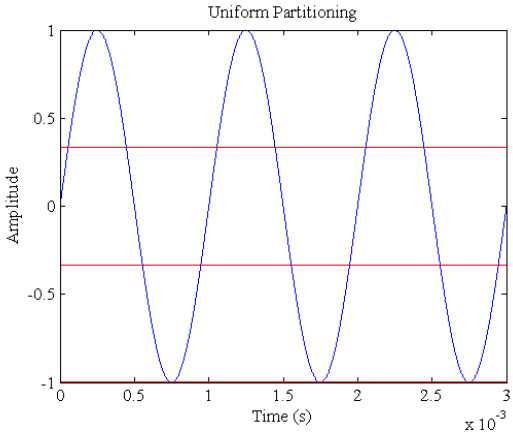

Figure 2. Example of uniform partitioning of a sinusoid.

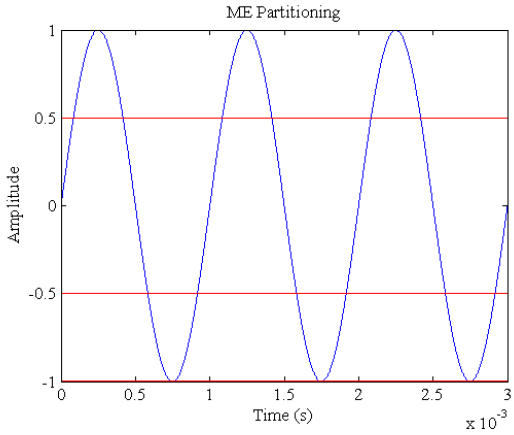

Figure 3. Example of ME partitioning of a sinusoid.

2.3.1. **ME Partitioning**

The maximum entropy (ME) partitioning scheme was defined by the principle of entropy in determining the partition structures. Recall entropy as shown in Eq. 1.

$$H(X) = -\sum_{i=1}^{n} p(x_i) \log_2 p(x_i) \qquad (1)$$

The entropy can be maximized by setting $p(x_i) = p(x_j), \forall i, j$. The logarithm to base 2 was used so that the unit of entropy is in bits. In the time series data, accomplishing maximization of entropy in the baseline case was necessary to make sure all partitions (or symbols) have equal probability of occurrence. The partition structure resulting from ME does not necessitate equal partitions as in the uniform case but does guarantee equal prior probabilities for the partitions in the baseline case. A feature of the ME partitioning scheme is that the partitions boundaries are closer in regions of the data where there are a dense number of data points. In regions where there are fewer date points, fewer partitions are generated in these areas. An example of ME partitioning on a sinusoidal signal is shown in Figure 3. For the ME case, the resultant probability of the symbols was equal compared to uniform partitioning whereas the partition regions are equal in size with unequal symbol probabilities.

Once the partitions are defined each partition was labeled with a symbol from the alphabet *S*. Given a time series *X* of length *M*, if $x_i \in P_i, 0 \leq i \leq M$, then assign $s_i \rightarrow x_i, \forall i;\ s_i \in S$. By implementing the partition structure and assigning a unique symbol to each time series date point, the end result was called the symbol stream. This is the re-quantized time series data that is now transformed into the symbolic domain.

2.4. **Statistical Model Development**

Once the partitions have been developed and symbols assigned to each partition, the next step is to construct the statistical model based on the resultant symbol stream. This step consists of another parameter for the SA methodology, the depth parameter *D*. The depth parameter controls the definition of model states. States in the model are formed from *D*-length subsets of symbols. Therefore, the total number of states in the algorithm given the number of partitions *P* and the depth *D* is shown in Eq. (2).

$$N_s = P^D \qquad (2)$$

As an example, assume a ternary partition scheme is implemented that results in three symbols; labeling them -1, 0, and 1. The methodology's resultant statistical states depend on the number of symbols in the algorithm as well as the chosen depth. The parameter depth adjusts the memory of the resultant symbolic model, that is, the parameter controls the groupings of symbols into states. For instance, if *D* was unity, the resultant states are 0, 1, and -1. If *D* was two, the resultant states would be 00, 01, 10, 11, 0-1, (-1)0, (-1)(-1), 1(-1), and (-1)1 according to (2).

Shown in Figure 4 is an example of the method continuing the above example with the three partition symbolic system with *D* being equal to two applied to a recorded sine wave of arbitrary amplitude. The number of resultant states is equal to three. The example sine wave in the figure is divided into zero (0), one (1) or minus one (-1) by a set threshold (partition boundary). The resultant square wave like symbol waveform developed by the processor or field programmable gate array (FPGA) is shown in the figure. The FGPA then counts the state occurrences which can then be converted into probabilities to generate what is known as the State Probability Vector (SPV).

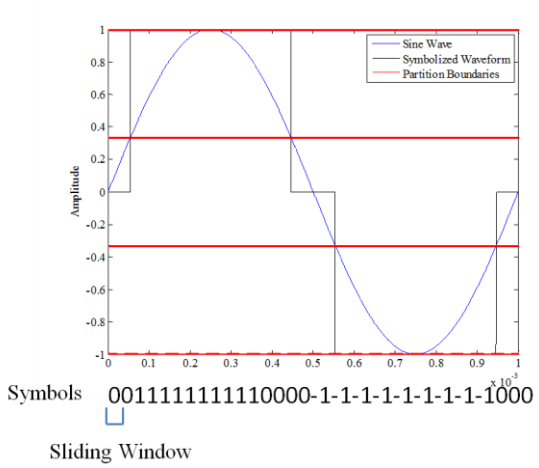

Figure 4. Example symbolization using three symbols with *d*=2 resulting in nine possible states.

With the symbol sequence s_i completed, the next step is to form states out of the symbols or groups of symbols. The probabilities of the state occurrences can be calculated and tracked across each data capture. These probabilities are arranged in a $N_s x1$ vector, where N_s represents the total number of states in the algorithm given by Eq. (2), which is the SPV. In the case where depth of the algorithm is equal to unity, as it is with most cases, the total number of states is equal to the number of symbols used. Choosing *D* equal to unity results in the smallest possible model for a given number of symbols thereby reducing computational complexity of the approach.

In addition to tracking the probability of the model states, the transition probabilities can also be calculated. The transition matrix captures the dynamics of the symbolic model and it is possible to calculate the SPV given the state transition matrix as shown in Eq. (3).

$$v_i \Pi = \lambda_i v_i \qquad (3)$$

In Eq. (3), Π is the state transition matrix, λ_i is the i^{th} eigenvalue equal to unity, and v_i is the left eigenvector of Π associated with the unity eigenvalue. Using the examples in Figure 2 and Figure 3, the state transition matrices are shown in **Table 1**.

Table 1. Example state transition matrices for uniform and ME partitioning.

Uniform Partitioning – Π Matrix		
0.99847	0.00153	0.00000
0.00278	0.99445	0.00278
0.00000	0.00153	0.99847
ME Partitioning – Π Matrix		
0.99820	0.00180	0.00000
0.00180	0.99640	0.00180
0.00000	0.00180	0.99820

Both of the matrices show little change between either types of partitioning. The results display strong diagonal terms as would be expected with symbolic analysis and with sinusoidal data. From the natural progression of the sinusoidal data, it is evident that there would be no instantaneous transitions between the minimum and maximum values resulting in the two zero transitional probabilities. The SPVs for each type of partitioning is shown in **Table 2**.

Table 2. Example SPV for Uniform and ME Partitioning.

Uniform Partitioning
0.392
0.216
0.392
ME Partitioning
0.333
0.333
0.333

The difference between uniform and ME initial SPVs can be observed in the above table. As was mentioned earlier, uniform partitioning results in equal partition sizes but not equal state probabilities. The opposite is true with ME partitioning with the resultant state probabilities equal but the partition sizes are not.

Once the probabilities or counts as shown in Table 2 are known, a distance type metric can be applied to the baseline case and future cases to develop an anomaly based on the current system operation. More deviation from this baseline will translate into a measureable anomaly at the algorithm's output.

2.5. **Anomaly Generation**

Anomalies inherent to degradation in the system can be generated from the use of the SPV between the data captures. The metric quantifies the deviation between the

known baseline, commonly known as the healthy state of the system, and a future system state. A measure commonly used to quantify an anomaly between captures is based on the Manhattan distance given in Eq. (4).

$$A = \left\| z_{nominal} - z_j \right\|_1 \quad (4)$$

In Eq. (4), $z_{nominal}$ is the nominal (baseline) SPV and z_j is the SPV at iteration j. From this measure, it is possible to quantify anomalies present in the system and how they evolve over time and usage. For the state transition matrix anomaly measure, the Frobenious norm of the difference between two state transition matrices can be used. From this evolution of the anomaly, it is then possible to define a threshold of failure for the system. The threshold can then be implemented in a predictor to estimate remaining useful life of the system.

The anomaly can be used as a diagnostic measure to determine the amount of degradation the system has incurred over its lifetime or to be used as a prognostic measure. If training data exists for the system, the anomaly measure can then be used in a prognostic application to predict the remaining useful life of the system.

3. SYNTHETIC APERTURE RADAR

The focus of the effort was in applying the Symbolic Analysis health management approach to SAR platforms. These platforms are imaging based radars that operate in frequency ranges up to the 10s of GHz. While the methodology is applicable to many systems aboard remotely piloted aircraft, the SAR platform was targeted for this research because of its importance to missions as well as the high cost of maintenance and repairs. A health methodology such as the one based on SA can reduce these costs dramatically.

The imaging radar works by mathematically assuming that a series of radar pulses and returns were generated and measured by a single large radar antenna (synthetic aperture) (Richards, Scheer, & Holm, 2010). In order to operate, the platform must be travel some finite distance during the pulse intervals.

The radar class investigated was the Active Electronically Scanned Array (AESA) radar (Melvin & Scheer, 2013). The radar itself is made up of hundreds of smaller transmit/receive (T/R) modules. Each one of these modules contains the necessary electronics for transmitting and receiving radar pulses. The T/R modules also contain the phase control block which in combination with all the other modules allows the array to electronically scan.

An example block diagram of a T/R module is shown in Figure 5. The T/R Module contains dual channels for both receiving reflections as well as for transmitting. Common to the two paths is the phase shifter for each individual element to steer the beam. The attenuator is used to add an amplitude taper to the overall array to improve the transmit characteristics. Two switches are used to select transmit and receive channels as necessary. The transmit path consists of the driver and power amp to gain the signal to the antenna element. The power is sent to the antenna through SW2 which is typically a circulator. Switching the channel to receive, the first element is the Low Noise Amplifier (LNA) with a pre-amplifier filter. The diode on the input is used to protect the LNA and for impedance matching.

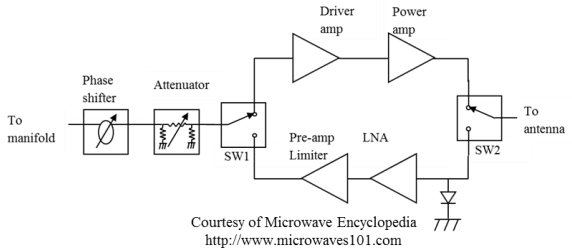

Figure 5. Example block diagram of a T/R module for an AESA radar element.

A general imaging SAR diagram is shown in Figure 6. The cross-range resolution of SAR imagery is dependent on the number of pulses sent out by the platform used in the image formation. The cross-range of a SAR image is the direction in line with the flight path of the radar system. The range direction is that which is perpendicular to the flight path. To increase range resolution, a wide bandwidth pulse is needed which would in turn require a short pulse emitted from the radar system as this short pulse would have wide bandwidth. However, to get enough signal power out such that echoes are detectable, a large instantaneous power is required which is currently unattainable with current solid-state transmitters. Instead, a frequency chirp is used so that lower instantaneous power can be used. In order to further improve the range resolution of the chirp, the resultant frequency chirp is pulse compressed.

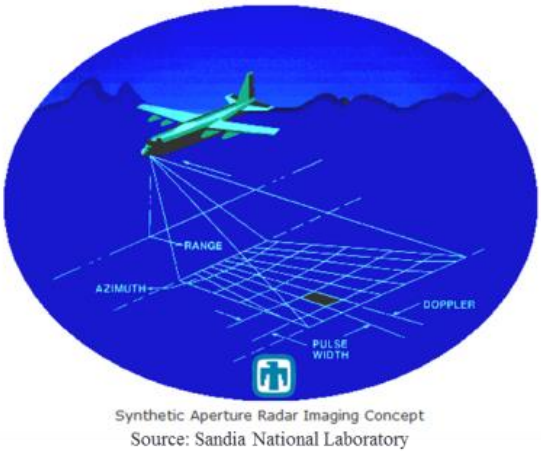

Figure 6. SAR radar imaging concept diagram.

Two types of degradation to radar images were simulated for the analysis. These events were jamming, classified as an external degradation event, and array degradation which is an internal degradation event. Both were simulated for the symbolic analysis routine. The results of these simulations were then used as input for the SA algorithm. The degradation simulations were developed to model electronic counter measures as well as deterioration effects.

The data readily available from AFRL's Sensor Data Management System (SDMS) was in the form of phase history. The phase history data is complex with both I and Q, containing both magnitude and phase of the echoes received at the radar. The phase history is calculated from the raw echo samples by using known platform related constants (flight path, etc.) and scaling (range scaling). The result is a phase history data matrix containing all N_P pulses sent from the transmitter with N_S samples per pulse. The symbolic algorithm operates on each column of the phase history matrix resulting in N_P iterations of the algorithm. The algorithm parameters must be chosen appropriately considering the number of samples available for processing and for probability convergence.

The phase history data implemented in this work was from the 2D/3D Imaging Gotcha Data Challenge ('Gotcha' dataset). This data contains phase history over 360° of azimuth of an urban environment consisting of numerous vehicles, roads, and other targets. Each degree of azimuth incorporates approximately 117 pulses with 424 frequency samples per pulse. The data was collected in the X-band (7 – 11 GHz) with a 640 MHz bandwidth. The data contains H/H, H/V, V/H, and V/V (transmit/receive) polarizations where H is horizontal and V is vertical. The different polarizations enable additional details about targets to be extracted from the reflected signals. An example from the Gotcha dataset is shown in Figure 7. The image was formed from 5° of azimuth resulting in a cross-range resolution of 0.19 m and a range resolution of .24m. The scene size is approximately 102 m by 108 m.

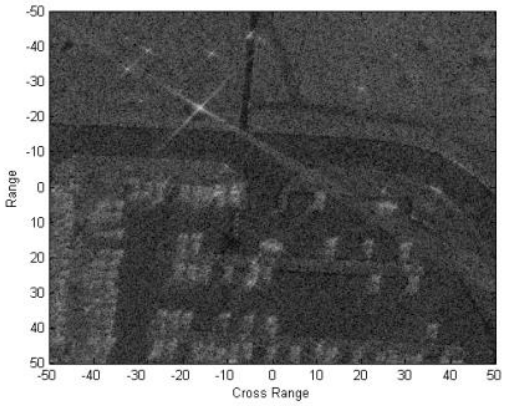

Figure 7. Example Gotcha SAR image.

The image of the parking lot located in the scene is shown in Figure 8 with the ground truth for the image in Figure 7 is shown in Figure 9**.** Figure 8 shows a view of the parking lot contained within the Gotcha scenes while Figure 9 shows the ground truth for the entire scene. The image in Figure 7 used the back projection algorithm for image generation (Gorham, & Moore, 2010). Additional photographs for the environment and targets can be found with the Gotcha Data Set (GOTCHA, 2011).

Figure 8. Parking lot image for Gotcha radar data.

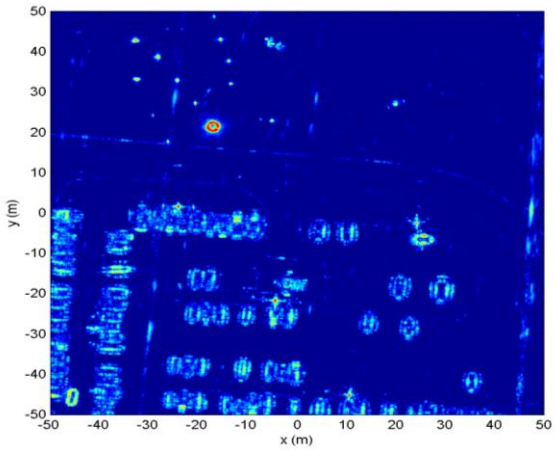

Figure 9. Gotcha ground truth.

4. RESULTS

In the Phase I work, the algorithm was simulated in a MATLAB environment investigating the SA response to both jamming and array degradation mechanisms. This section describes the approaches used to simulate the two degradation mechanisms as well as the results from the algorithm. The objective of each simulation was to determine the output of the SA algorithm to the degradation mechanisms presented in the data. In this manner, the output of the SA algorithm could also be used to intelligently classify the type of degradation (or mixture thereof) present within the system.

4.1. Jamming Degradation

The first type of degradation simulated was for radar jamming attacks. Jamming attacks are electronic countermeasures deployed to confuse or disrupt the normal operation of radar systems. There are two main types of jamming, one is related to denial of operation and the other is false target injection.

False target jamming uses an intelligent transceiver in which the source radar is monitored, manipulated, and re-transmitted. The re-transmitted signals can be used to obscure the location of ground-based objects or introduce false targets in the radar system. This type of attack falls under what is known as Digital Radio Frequency Memory (DRFM) (Kwak, 2009)(Mehalic, & Sayson, 1992)(Berger, 2001). This type of attack learns the behavior of the source radar and transmits a manipulated signal back to the receiver. The other type of attack implementing DRFM is the denial of operation. A ground based or other receiver learns the transmitted characteristics of the source radar and transmits noise at those frequencies. The transmitted noise then significantly reduces the ability to resolve objects in the image produced through SAR mapping.

Mathematically, Gaussian noise is given in Eq. (5) shown below.

$$N(\mu,\sigma) = \frac{1}{\sqrt[2]{2\pi\sigma^2}} e^{-\frac{(x-\mu)^2}{2\sigma^2}} \qquad (5)$$

In order to simulate a jamming attack and inject the additive Gaussian noise into the system, the parameters μ and σ^2 (mean and variance) must be known. These parameters are estimated from the radar data and considered as the healthy non-degraded parameters. With the parameters defined, the noise is added into the system as shown in Eq. (6).

$$PH_{corrupted} = PH_{original} + N(\alpha\mu_0, \alpha\sigma_0) + jN(\alpha\mu_0, \alpha\sigma_0) \qquad (6)$$

In (6), PH is the Phase History, α is a scalar, and $N(\mu,\sigma)$ is the additive Gaussian noise. Note that in Eq. (6), the noise is added to both the real and imaginary components of the PH. Each additive noise component is independent of each other. The scalar, α, is defined in Eq. (7).

$$\alpha = 10^{\frac{P(dB)}{20}} \qquad (7)$$

The parameter controls the strength of the jamming attack such that if P(dB) = 0, the Signal-to-Noise Ratio (SNR) of the resultant system would be 0 dB. The resultant power of the jamming noise would equal to that of the returned echoes.

The jamming corruption was then implemented on the Gotcha data set. In this case, $P(dB)$ was chosen to be 0 dB. The estimated noise parameters are shown in Table 3.

Table 3: Estimated Noise Parameters from Gotcha Radar Data

Estimated Noise Parameters from Radar Data		
	Real	**Imaginary**
Mean, μ	2.450e-7	8.373e-8
Variance, σ_v^2	6.461e-4	6.461e-4

This results in the scalar, α, having the value of unity. The resulting image is shown in Figure 10**.**

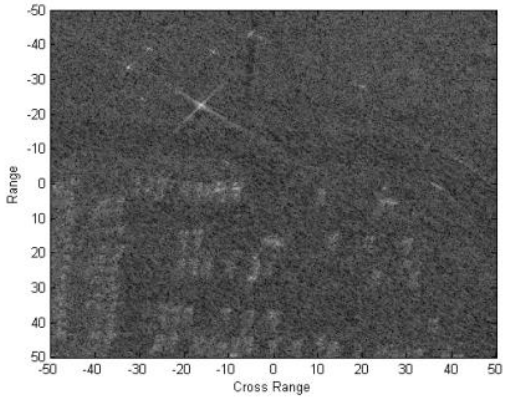

Figure 10. Jamming corruption: Gotcha SAR image.

Compare the results of Figure 10 to those in Figure 7 which contain the original image. As anticipated, the jamming significantly reduces the ability to resolve objects in the image. The stronger reflections in the scene due to metallic objects can still be seen due to the starburst effect; however, the details of the road and parking lot are significantly reduced.

The PH data with the included jamming noise was then implemented in the SA algorithm. The parameters used in the analysis are shown in **Table 4.**

Table 4: SDAAD Parameters for ME and Uniform Partitioning – Jamming

Parameters	**Number of Partitions**	**Depth**	**Resultant Number of States**
Uniform Partitioning	6	1	6
Maximum Entropy	6	1	6

For all of the following results, the SA routine was implemented on the magnitude of the PH data. The magnitude was chosen as it would represent any change between both the real part and the imaginary component of the PH. Other features that could be used are the individual

real or imaginary components or the angle between the real and imaginary components.

4.1.1. **Jamming – Uniform Partitioning**

The first set of results was developed with uniform partitioning. The resultant anomaly for the uniform partitioning jamming attack is shown in Figure 11. Recall that the signal to noise ratio (SNR) of this system was simulated to be 0dB in order to simulate a significant strength jamming attack to the radar platform.

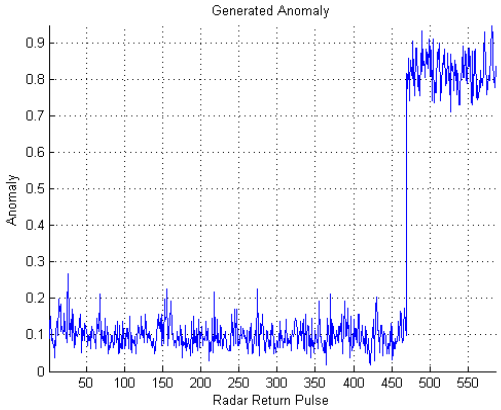

Figure 11. Jamming corruption: anomaly results – uniform partitioning.

In the figure, the jamming attack is clearly seen in the last 117 pulses of the image. In addition, the effects of jamming on these pulses, which represent about 20% of the total image, were shown in Figure 10. If the entire group of return pulses had been jammed, the image would have been totally corrupted but in order to demonstrate the change from a jammed pulse to a non-jammed pulse only the last 117 return pulses were jammed. The resulting anomaly has a magnitude of about 0.85. A threshold could be implemented around an anomaly magnitude of 0.8 to detect this type of degradation.

4.1.2. **Jamming – ME Partitioning**

The resultant anomaly magnitude formed from the state probabilities using the anomaly measure is shown in Figure 12.

Comparing these results to those obtained from the uniform partitioning, they are both similar in that both partitioning methods detect the added jamming noise at the instance it was injected. The resultant magnitude of the anomalies is also comparable at about 0.85. A notable difference is in the anomaly measure before the jamming. As can be observed in the ME partitioning, the anomaly is slightly larger.

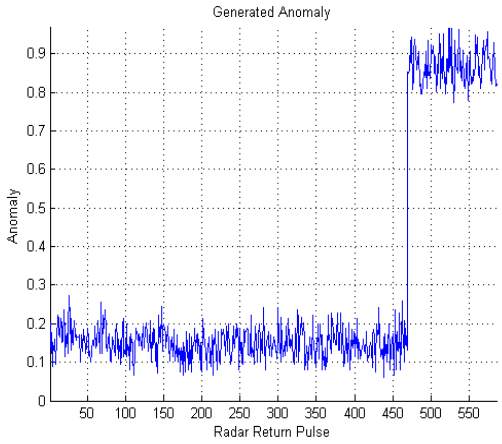

Figure 12. Jamming corruption: anomaly results – ME partitioning.

Recall that ME partitioning results in partition structures that finely divide dense regions of data and coarsely divide sparse regions. This also results in equal initial partition probabilities and hence symbol probabilities that evolve with degradation. Due to this distribution, any small deviation, either from degradation or environment, can be detected by this partitioning methodology. Figure 12 shows a slightly larger anomaly magnitude which is a result of slight differences in data between pulses. This slight increase may be problematic when the approach is applied to a data from a fielded system. Because of this, uniform partitioning may be the most appropriate partition approach for future work.

4.2. **Array Degradation**

Array degradation was the next type of degeneration that was simulated. This type of degradation represents internal platform degradation and was also implemented using the SAR Gotcha dataset. From the T/R module (Figure 5), there are two paths within each array module. The weakest link in each module is the power amplifier used as the final stage to drive the antenna. It was assumed in this analysis the amplifier fails such that the module can no longer transmit. Since the receive path is still intact, it is assumed that the module can receive echoes.

If the amplifier fails and the receive path is still active the overall transmit power decreases but the receive gain remained the same. It is known that the output power of an array degrades according to Eq. (8) (Rutledge, Cheng, York & Weikle, 1999).

$$dB_{LOSS} = 20log_{10}(1-\beta) \qquad (8)$$

The total transmit power loss can then be related to the percentage of failed elements β. The received power derived from the radar range equation is given in Eq. (9) (Richards et al, 2010).

$$P_r = \frac{P_t G_t G_r \lambda^2 \varepsilon}{4\pi^3 R^4} \quad (9)$$

In (9), P_t is the power transmitted, G_t is the gain of the transmit antenna, G_r is the gain of receive antenna, λ is the carrier wavelength, ε is related to the target's radar cross section (RCS), and R is the range to the target. In normal radar operation, the same antenna receives and transmits resulting in the same gain. However, the loss in transmit power can be modeled by applying a scalar directly to G_t which then directly results in a decrease in the received power since it is assumed that the receiver gain remains constant due to the fact that all elements can functionally receive echoes.

The transmit gain during the degradation simulation is shown in Figure 13**.** As was done with the jamming simulation, the array degradation was applied to 117 individual pulses on a single degree of azimuth. In this manner, each pulse was scaled by the values of the linear relationship shown in Figure 13.

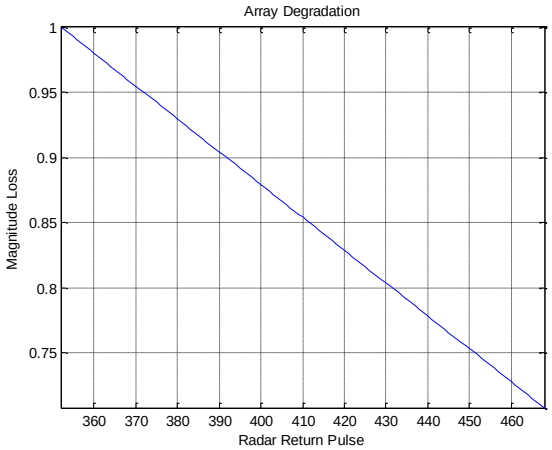

Figure 13. Array degradation simulation: Transmit gain plot, G_t for use in Eq. (9).

The scaling in the figure results in an applied -3 dB transmit loss to the antenna. This level was chosen as it is considered the failure point for a transmitting antenna. A 3dB loss translates to approximately 29% of the element modules failing in the array. An image formed from a simulated degraded array is shown in Figure 14.

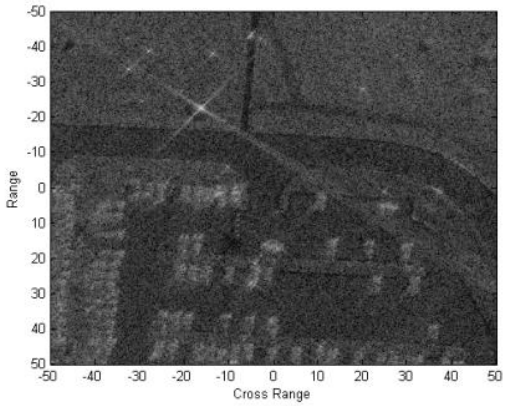

Figure 14. Array degradation: Gotcha SAR image.

The image degradation is minimal compared to the original non-degraded image shown in Figure 7. The image details of the parking lot can still be seen in the degraded image including the roadways and parked vehicles. For the SA analysis, the parameters implemented are shown in Table 5. The parameters implemented were the same as was implemented in the jamming simulation.

Table 5: SDAAD Parameters for ME and Uniform Partitioning – Array Degradation

Parameters	**Number of Partitions**	**Depth**	**Resultant Number of States**
Uniform Partitioning	6	1	6
Maximum Entropy	6	1	6

4.2.1. **Array Degradation – Uniform Partitioning**

The resultant anomaly formed from the deviation of these states from the baseline is shown in Figure 15. The figure shows the increasing anomaly that follows the degradation profile simulated. Note that the return pulse numbers in Figure 13 coincide with the algorithm output return pulse numbers in Figure 15.

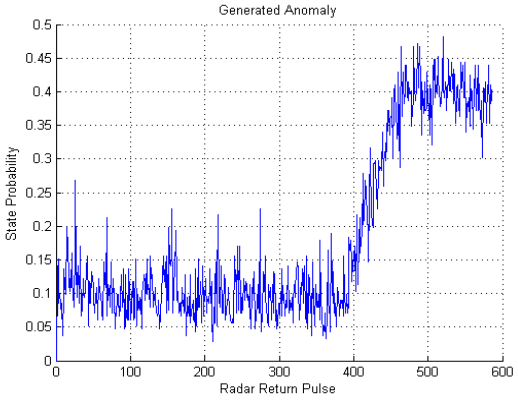

Figure 15. Array degradation: anomaly results– uniform partitioning.

For this simulation, the degradation profile was simulated on the second to last azimuth angle again applied to 117 pulses. The last azimuth angle was maintained at the -3dB degradation level. The increase in anomaly is observable and when the degradation is constant, the resultant anomaly is constant as well. The result also demonstrates the possibility of implementing a remaining useful life predictor on this type of degradation. This would assume that the array would degrade slowly over its useful life before needing to be pulled from the platform for repair. Through these simulations, the anomaly magnitude from a jamming event resulted in a larger anomaly magnitude which was due to the simulation. For example, weaker jamming attempts or more array degradation could result in comparable anomaly magnitudes. In future work these situations will be resolved by the classifier stage. In addition, the past history of the algorithm output can be used to discriminate between wear-out phenomenon in the array and deliberate platform jamming.

4.2.2. **Array Degradation – ME Partitioning**

The resultant anomaly formed from the same simulation using ME partitioning is shown in Figure 16**.**

As was done with the simulation under uniform partitioning, the degradation was applied to the second from the last azimuth degree so that the final degree could be held at the -3dB array degradation level. The resultant anomaly plot was similar to that obtained with uniform partitioning and the resultant magnitudes are also comparable. In this case, the -3dB anomaly magnitude is only slightly larger due to the larger nominal anomaly from pulses 1 through 400 (~0.15 for ME to ~0.10 for Uniform).

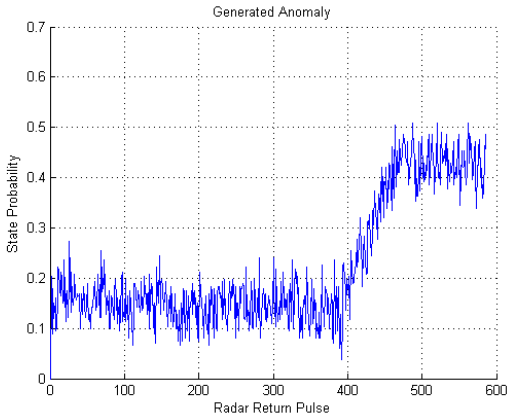

Figure 16. Array degradation: anomaly results – ME partitioning.

This result was also observed with the jamming results of the previous section. The difference is slight and the resultant responses from the partitioning methods remain similar. Since the results are similar, the application of this approach to SAR platforms would dictate that either partitioning method could be implemented. Obtaining more data from fielded system may give more insight into which approach would be more applicable for degradation monitoring. From this initial research, although the results are positive in general, a determination of which partitioning methodology is superior to the other cannot be stated.

5. **COMBINED DEGRADATION**

Separate degradation mechanisms such as those above can be easily identified when they occur by themselves. More interesting is the case when multiple degradation mechanisms occur simultaneously. For this reason, the two degradation mechanisms above were simulated simultaneously with the effects superimposed in the data. For instance, the array was first degraded by applying the degradation to the second from the last azimuth angle of data and holding the last angle of data at -3dB degradation. At this point, a jamming attack was simulated on top of the array degradation.

In this case, the parameters for the test were, six partitions, depth of unity, and the partitioning method was uniform. In this case, uniform was arbitrarily chosen since each approach yielded similar results in the previous analysis. The resultant SAR image formed from the combined degradation is shown in Figure 17. As with previous simulations, the jamming power was again set to 0dB.

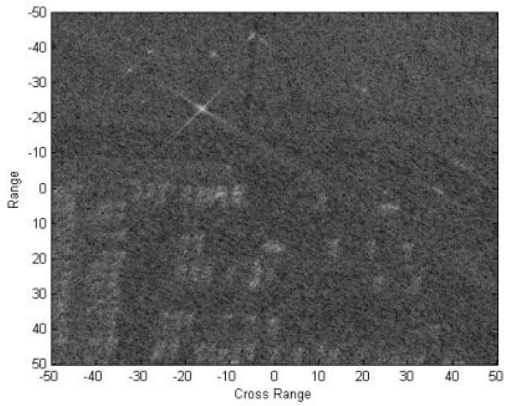

Figure 17. Combined degradation: Gotcha SAR.

In the image, the degradation is observable with the jamming being the strongest source of degradation. Compare this image to that obtained from jamming only, Figure 10. The two images look similar with Figure 17 showing slightly more image degradation. The resultant anomaly from this combined effect is shown in Figure 18.

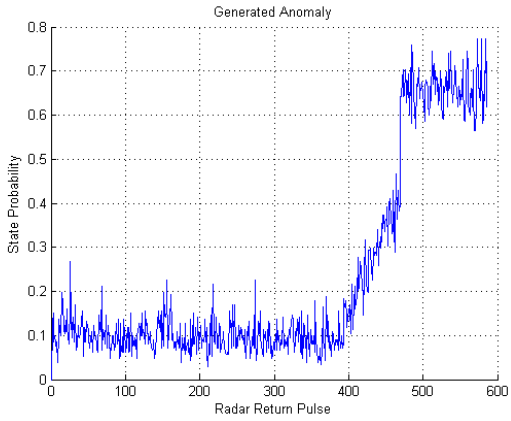

Figure 18. Combined degradation: anomaly results– uniform partitioning.

The results in Figure 18 show a distinct combination of the two degradation effects. In pulses 400 through 480, the array degradation is clearly seen. In pulses 480 through 580, the combined effects of jamming and array degradation are seen although the strength of the jamming attack overcomes that of array degradation and manifests itself as a discontinuity in the anomaly magnitude. The discontinuity that arises from jamming attacks could be implemented in the degradation classifier and assist in determining whether degradation is internal or external.

6. CONCLUSION AND FUTURE WORK

The method of Symbolic Analysis was demonstrated using simulated degradation in SAR phase history data. Under a MATLAB environment, both jamming and array degradation were simulated and the results observed. The simulations analyzed the results from both uniform and maximum entropy partitioning methods under the same number of partitions and algorithm depth. The data used was phase history data that was corrupted with degradation representing jamming and array failure events. Once corrupted, the magnitude of this data was used as the input into the SA algorithm. The results show similarities between the two with ME being slightly more sensitive to the data as compared to uniform. In addition, the results were simulated with combined degradation mechanisms. In these cases, it was shown that it is possible to perform classification on the resultant algorithm output such that degradation can be identified. From these initial results, it seems to be the case that uniform partitioning would be preferable to ME to reduce the probability of false positives.

QorTek has been awarded a Phase II research program to expand the methodology and apply to both healthy and degraded field data from imaging radars. The new research project will investigate the results of the Phase I to validate the simulations as well as to expand the number of degradation mechanisms to model. Another objective of this research is to expand on the degradation classification as well as investigate the application of prognostics to the approach. QorTek plans to also use this research to definitively determine if there is a superior partitioning methodology between the two presented in the initial work. In addition, the Phase I work only investigated using the magnitude and not the angle of the complex data. The Phase II work will investigate using additional features and using the partitioning approach to generate a one-dimensional symbolic data set. It is anticipated that the algorithm will be implemented and a prototype flight-tested on a SAR radar payload.

The output of the SA can be utilized in a prognostic application. The output of the algorithm would provide a measurement of degradation which would act as an input for a Kalman-type predictor. As was observed, the output of the algorithm is related to the amount of degradation sustained by the radar. Since the exact evolution of the radar faults are not exactly known, a generic model must be implemented for the Kalman filter. A kinematic-motion model could be applied for the Kalman model. Future work will also address the determination of how much degradation can be sustained by the payload until it is deemed 'failed.' This work is anticipated to be carried out in the Phase II program.

ACKNOWLEDGMENTS

This work was funded by the US Air Force under contract FA8650-11-M-3138. QorTek would like to express our thanks to Thierry Pamphile from RQQI and Dale Kristof from WIIE for their support during this SBIR work. QorTek would also like to acknowledge the assistance

from LeRoy Gorham, RYAPX, Wright-Patterson Air Force Base. His help with SAR image processing is greatly appreciated.

NOMENCLATURE

A	=	anomaly
α	=	noise scaling constant
β	=	percentage of failed array
D	=	symbolic depth
$H(\cdot)$	=	entropy
M	=	time series data length
N_s	=	number of states
$p(\cdot)$	=	probability
P_i	=	i^{th} partition
s_i	=	i^{th} symbol
U	=	time series data amplitude range
X	=	time series data
z	=	state probability vector
v_i	=	i^{th} eigenvector
λ_i	=	i^{th} eigenvalue
Π	=	state transition matrix

REFERENCES

Bower, G., Mayer, J., & Reichard, K. (2011). "Symbolic Dynamics and Analysis of Time Series Data for Diagnostics of a dc-dc Forward Converter," in *Annual Conference of the Prognostics and Health Management Society*, Montreal, 2011.

Bower, G., Mayer, J., & Reichard, K. (2008). "Symbolic Dynamics for Anomaly Detection in a dc-dc Forward Converter," *Proceedings of the 2008 International Conference on Prognostics and Health Management*, Denver, October 2008.

Berger, S. D. (2001). "The spectrum of a digital radio frequency memory linear range gate stealer electronic attack signal," *Proceedings of the 2001 IEEE Radar Conference*, Atlanta, 2001.

Daw, C.S., C.E.A. Finney & E.R. Tracy (2003). "A review of symbolic analysis of experimental data." Review of Scientific Instruments 74.2 (2003): 915-930.

Gorham, L. & L. Moore (2010). "SAR image formation toolbox for MATLAB." *Proceedings of the SPIE*. 2010.

Kwak, C.M. (2009). "Application of DRFM in ECM for pulse type radar," *34th International Conference on Infrared, Millimeter, and Terahertz Waves*, Busan, Korea, 2009.

Mehalic, M. & Sayson, A. M. (1992). "A dual-port DRAM component for a digital RF memory," *Proceedings of the IEEE 1992 National Aerospace and Electronics Conference*, Dayton, 1992.

Melvin, William L., Scheer, James, A. (2013). *Principles of Modern Radar: Advanced Techniques*. Edison, NJ: SciTech Publishing.

Papoulis, A., & Pillai U. S. (2002). *Probability, Random Variables, and Stochastic Processes.* 4th Edition, New York, NY: McGraw-Hill.

Ray, Asok (2004). "Symbolic dynamic analysis of complex systems for anomaly detection." *Signal Processing* (2004): 1115-1130.

Richard, Mark A., Scheer, James A., & Holm, William A. (2010). *Principles of Modern Radar: Basic Principles*. Raleigh, NC: SciTech Publishing, Inc.

Rutledge, D., Cheng, N., York, R. & Weikle II, R. (1999). "Failure of Power Combining Arrays." *IEEE Transactions on Microwave Theory and Techniques* 47.7 (1999): 1077-1082.

U.S. Air Force. Gotcha Volumetric SAR Data Set. Sensor Data Management System. August 2011. <https://www.sdms.afrl.af.mil/index.php?collection=gotcha>.

BIOGRAPHIES

Gregory Bower received his B.S., M.S, and Ph.D. degrees all from the Pennsylvania State University. He is currently the Chief Technology Officer for QorTek, Inc. where he focuses on diagnostic and prognostic methods and power electronic design and development. Previously, he was a research assistant for the Applied Research Laboratory in State College, PA. His research interests include Prognostics and Health Management (PHM) of electronic systems, statistical methods, robust and optimal control theory, system identification, and power conversion. He is a member of Eta Kappa Nu, Tau Beta Pi, and IEEE.

Jonathan Zook received a B.S. in Electronics Engineering from Pennsylvania State University. Jonathan is the Engineering Manager of QorTek, Inc. responsible for helping to oversee innovative projects on the cutting edge of power electronics design. His research interests include high speed parallel processing, digital control of high efficiency power converters and amplifiers for smart material actuators. He is a member of the IEEE.

Ross Bird received his B.S. in Electronics from Penn State in 2001 and received his MSEE in 2003. He is currently the president of QorTek, Inc. since 2010. He has worked extensively at the leading edge of power electronics design holding several patents that incorporate advanced materials, design and digital control within these systems. His research interests include wide bandgap power electronics and devices, high efficiency power conversion, extremely high density power electronics, smart materials systems, and piezoelectronics. He is a member of the IEEE.